
DRAFT

CMS Paper

The content of this note is intended for CMS internal use and distribution only

2009/07/24

Archive Id: 1.3

Archive Date: 2009/07/24 17:01:07

Measurement of the Dijet Mass Distribution and Search for New Particles in pp Collisions at 10 TeV

The CMS Collaboration

Abstract

We present an early paper draft, which contains only simulation and theory, but what follows is written as if it were reporting a real measurement of early CMS data.

We have used 10 pb^{-1} of integrated luminosity from the CMS experiment at the Large Hadron Collider at CERN to search for new particles decaying to dijets. The measured dijet mass spectrum agrees with QCD predictions. We exclude at the 95% confidence level models containing the following new particles: axigluons and flavor universal colorons with mass below $1.8 \text{ TeV}/c^2$, excited quarks with mass below $1.9 \text{ TeV}/c^2$ and E_6 diquarks with mass below $1.0 \text{ TeV}/c^2$ and within the range $1.3\text{--}1.8 \text{ TeV}/c^2$.

This box is only visible in draft mode. Please make sure the values below make sense.

PDFAuthor:	Robert Harris, Chiyoung Jeong, Kostas Kousouris, Sung-Won Lee, Sertac Ozturk
PDFTitle:	Measurement of the Dijet Mass Distribution and Search for New Particles in pp Collisions at 10 TeV
PDFSubject:	CMS
PDFKeywords:	CMS, physics, software, computing

Please also verify that the abstract does not use any user defined symbols

1 Within the standard model events with two energetic jets (dijets) are expected to arise in proton-
 2 proton collisions from parton-parton scattering. The outgoing scattered partons manifest them-
 3 selves as hadronic jets. The dijet mass spectrum predicted by Quantum Chromodynamics
 4 (QCD) falls smoothly and steeply with increasing dijet mass. Many extensions of the stan-
 5 dard model predict the existence of new massive objects that couple to quarks (q) and gluons
 6 (g), and result in resonant structures in the dijet mass spectrum. In this paper we report a search
 7 for narrow resonances in the dijet mass spectrum, measured with the Compact Muon Solenoid
 8 (CMS) detector at the CERN Large Hadron Collider, at a proton-proton collision energy of
 9 $\sqrt{s} = 10$ TeV.

10 In addition to this generic search, we specifically search for the following eight models of dijet
 11 resonances. First, in a model where the symmetry group $SU(3)$ of QCD is replaced by the
 12 chiral symmetry $SU(3)_L \times SU(3)_R$, there are axial vector particles called axigluons A which
 13 decay to $q\bar{q}$ [1]. Second, the flavor-universal coloron model also embeds the $SU(3)$ of QCD
 14 in a larger gauge group, and predicts the presence of a color-octet coloron C which decays to
 15 $q\bar{q}$ [2]. Third, if quarks are composite particles then excited states are expected, and we search
 16 for mass degenerate excited quarks q^* that decay to qg [3]. Fourth, grand unified theory based
 17 on the E_6 gauge group predicts the presence of scalar diquarks D and D^c which decays to
 18 $\bar{q}\bar{q}$ and qq [4]. Fifth, models of technicolor predict the presence of color octet technirhos ρ_T
 19 which decay to $q\bar{q}$ and gg [5]. Sixth, the Randall-Sundrum model of extra dimensions predicts
 20 massive gravitons G which decay to $q\bar{q}$ and gg [6]. Seventh and Eighth, models which propose
 21 new gauge symmetries often predict new gauge bosons W' and Z' which decay to $q\bar{q}$ [7].

22 A detailed description of the CMS experiment can be found elsewhere [8, 9]. The CMS coordi-
 23 nate system has the origin at the center of the detector, z -axis points along the beam direction
 24 toward the west, with the transverse plane perpendicular to the beam. We define ϕ to be the
 25 azimuthal angle, θ to be the polar angle and the pseudorapidity as $\eta \equiv -\ln(\tan[\theta/2])$. The
 26 central feature of the CMS apparatus is a superconducting solenoid, of 6 m internal diame-
 27 ter. Within the field volume are the silicon pixel and strip tracker, and the barrel and endcap
 28 calorimeters ($|\eta| < 3$): a crystal electromagnetic calorimeter (ECAL) and a brass-scintillator
 29 hadronic calorimeter (HCAL). Outside the field volume, in the forward region, there is an iron-
 30 quartz fiber hadronic calorimeter ($3 < |\eta| < 5$). The HCAL and ECAL cells are grouped into
 31 towers, projecting radially outward from the origin, for triggering purposes and to facilitate
 32 the jet reconstruction. In the region $|\eta| < 1.74$ these projective calorimeter towers have seg-
 33 mentation $\Delta\eta = \Delta\phi = 0.087$, and the η and ϕ width progressively increases at higher values
 34 of η . The energy in the HCAL and ECAL within each projective tower is summed to find the
 35 calorimeter tower energy. Towers with $|\eta| < 1.3$ contain only cells from the barrel calorimeters,
 36 towers in the transition region $1.3 < |\eta| < 1.5$ contain a mixture of barrel and endcap cells, and
 37 towers in the region $1.5 < |\eta| < 3.0$ contain only cells from the endcap calorimeters.

38 Jets are reconstructed using the seedless infrared safe cone algorithm with cone size $R =$
 39 $\sqrt{(\Delta\eta)^2 + (\Delta\phi)^2} = 0.7$ [10]. Below we will discuss three types of jets: reconstructed, cor-
 40 rected and generated. The reconstructed jet energy, E , is defined as the scalar sum of the cal-
 41 orimeter tower energies inside the jet. The jet momentum, \vec{p} , is the corresponding vector sum:
 42 $\vec{p} = \sum E_i \hat{u}_i$ with \hat{u}_i being the unit vector pointing from the origin to the energy deposition E_i
 43 inside the cone. The jet transverse momentum, p_T , is the component of \vec{p} in the transverse
 44 plane. The E and \vec{p} of a reconstructed jet are then corrected for the non-linear response of the
 45 calorimeter to a generated jet. Generated jets come from applying the same jet algorithm to the
 46 Lorentz vectors of stable generated particles before detector simulation. On average, the p_T
 47 of a corrected jet is equal to the p_T of the corresponding generated jet. The corrections estimated
 48 from a GEANT [11] simulation of the CMS detector increase the average jet p_T by roughly 50%

(10%) for 70 GeV (3 TeV) jets in the region $|\eta| < 1.3$. Further details on jet reconstruction and jet energy corrections can be found elsewhere [12, 13]. The jet measurements presented here are within the region $|\eta| < 1.3$, where the sensitivity to new physics is expected to be the highest, and where the reconstructed jet response variations as a function of η are both moderate and smooth.

The dijet system is composed of the two jets with the highest p_T in an event (leading jets), and the dijet mass is given by $m = \sqrt{(E_1 + E_2)^2 - (\vec{p}_1 + \vec{p}_2)^2}$. We require both leading jets have pseudorapidity $|\eta| < 1.3$. The estimated dijet mass resolution varies from 9% at a dijet mass of 0.7 TeV to 4.5% at 5 TeV. We use data from the 2009-2010 running period corresponding to an integrated luminosity of 10 pb^{-1} . The sample we use for this search was collected by requiring at least one jet in the high level trigger with $p_T > 110 \text{ GeV}/c$. The trigger efficiency, measured from a sample acquired with a prescaled trigger with a lower p_T threshold, was greater than 99% for dijet mass above $420 \text{ GeV}/c^2$. Backgrounds from cosmic rays, beam halo, and detector noise are expected to occasionally produce events with large or unbalanced energy depositions. They are removed by requiring $\cancel{E}_T / \sum E_T < 0.3$ and $\sum E_T < 10 \text{ TeV}$, where \cancel{E}_T ($\sum E_T$) is the magnitude of the vector (scalar) sum of the transverse energies measured by all calorimeter towers in the event. This cut is more than 99% efficient for both QCD jet events and the signals of new physics considered. In the high p_T region relevant for this search, jet reconstruction is fully efficient.

In Fig. 1 we present the inclusive dijet mass distribution for $p\bar{p} \rightarrow 2 \text{ leading jets} + X$, where X can be anything including additional jets. We plot the differential cross section versus dijet mass in bins approximately equal to the dijet mass resolution. The systematic uncertainty on the cross section arises predominantly from a 10% uncertainty on the jet energy correction, but also includes a 10% uncertainty on the luminosity. The data is compared to a prediction from PYTHIA [14] which includes a simulation of the CMS detector and the jet energy corrections. The data is also compared with a full QCD prediction at next-to-lowest order [15] convoluted with the dijet mass resolution of the CMS detector for corrected jets. Both predictions use CTEQ6 parton distributions [16] and a renormalization scale $\mu = p_T$. The data agrees with both predictions within the systematic uncertainties of the measurement. To test the smoothness of our measurement as a function of dijet mass, we fit the data with the parameterization

$$\frac{d\sigma}{dm} = \frac{P0[1 - (m/\sqrt{s}) + P3(m/\sqrt{s})^2]^{P1}}{m^{P2}} \quad (1)$$

with the four parameters $P0$, $P1$, $P2$ and $P3$. In Figs 2 we show both the data and the background fit, which has a χ^2 of 23 for 32 degrees of freedom. In Figure 3 we show the fractional difference between the data and the background fit. The data is well fit by the smooth parameterization and shows no evidence of new particles.

To set limits on dijet resonances it is sufficient to use the resonance line shape for only one new particle type assuming each new particle's natural half-width ($\Gamma/2$) is small compared to the dijet mass resolution. In Figs. 2 and 3 we show the predicted line shape for excited quarks (q^*) using the PYTHIA Monte Carlo [14] and a CMS detector simulation. The mass resolution has a Gaussian core from jet energy resolution and a long tail towards low mass from QCD radiation. We have used the q^* mass resonance curves in Figs. 2 and 3 to model the shape of all new particles decaying to dijets. We perform a binned maximum likelihood fit of the data to both the background parameterization and the signal hypothesis. The method gave a Poisson likelihood as a function of the signal cross section. This was done independently at 29 different values of new particle mass from 0.7 to 3.5 TeV/c^2 in 0.1 TeV/c^2 steps resulting in 29 statistical likelihood distributions from which we found initial 95% confidence level upper

limit on the cross section including only statistical uncertainties. Systematic uncertainties on the cross section limits are dominated by a 10% uncertainty in the jet energy scale. Variations in jet response to quarks and gluons made the cross section limit dependent on whether we chose a $q\bar{q}$ or gg resonance instead of our default qg resonance, and these variations were included as a systematic. The cross section limit also depended on the choice of background parameterization and uncertainties in the simulation of the dijet mass resolution. We combined these uncertainties in quadrature and convoluted each of the 29 Poisson likelihoods with the Gaussian systematic uncertainty and found the final 95% confidence level upper limits on the cross section presented in Table I.

In Fig. 4 we compare our measured upper limit on the cross section times branching ratio for a new particle decaying to dijets to the theoretical predictions. The predictions are lowest order calculations with CTEQ6L parton distributions [16] for dijets with $|\eta| < 1.3$. We exclude at 95% C.L. new particles in mass regions for which the theory curve lies above our upper limit. For axigluons (or flavor universal colorons) we exclude the mass range $0.7 < M(A) < 1.8$ TeV/ c^2 , extending the previous exclusions [17] of $120 < M(A) < 1250$ GeV/ c^2 obtained by the Tevatron. For excited quarks we exclude the mass range $0.7 < M(q^*) < 1.9$ TeV/ c^2 , extending the previous exclusions [17] of $260 < M(q^*) < 870$ GeV/ c^2 . For E_6 diquarks we exclude the mass range $0.7 < M(D) < 1.0$ TeV/ c^2 , and $1.3 < M(D) < 1.8$ TeV/ c^2 , extending the previous exclusions [17] of $290 < M(D) < 630$ GeV/ c^2 .

In conclusion, the measured dijet mass spectrum is a smoothly falling distribution which agrees with the predictions of the standard model. We see no significant evidence for new particle production and set limits on axigluons, flavor universal colorons, excited quarks, and E_6 diquarks.

We thank the technical and administrative staffs at CERN and other CMS Institutes, and acknowledge support from: FMSR (Austria); FNRS and FWO (Belgium); CNPq and FAPERJ (Brazil); MES (Bulgaria); CERN; CAS and NSFC (China); MST (Croatia); University of Cyprus (Cyprus); Academy of Sciences and NICPB (Estonia); Academy of Finland, ME and HIP (Finland); CEA and CNRS/IN2P3 (France); BMBF and DESY (Germany); GSRT (Greece); NKTH (Hungary); DAE and DST (India); IPM (Iran); UCD (Ireland); INFN (Italy); KICOS (Korea); CINVESTAV, CONACYT and UASLP-FAI (Mexico); PAEC (Pakistan); SCSR (Poland); FCT (Portugal); JINR (Armenia, Belarus, Georgia, Ukraine, Uzbekistan); MST and MAE (Russia); MSEP (Serbia); OCT (Spain); ETHZ, PSI, University of Zurich (Switzerland); NSC (Taipei); TUBITAK and TAEK (Turkey); STFC (United Kingdom); DOE and NSF (USA).

References

- [1] P. H. Frampton and S. L. Glashow *Phys. Lett.* **B190** (1987) 157.
- [2] E. H. Simmons *Phys. Rev.* **D55** (1997) 1678.
- [3] U. Baur, I. Hinchliffe, and D. Zeppenfeld *Int. J. Mod. Phys.* **A2** (1987) 1285.
- [4] J. L. Hewett and T. G. Rizzo *Phys. Rept.* **183** (1989) 193.
- [5] K. Lane and S. Mrenna *Phys. Rev.* **D67** (2003) 115011.
- [6] L. Randall and R. Sundrum *Phys. Rev. Lett.* **83** (1999) 4690.
- [7] E. Eichten, I. Hinchliffe, K. D. Lane, and C. Quigg *Rev. Mod. Phys.* **56** (1984) 579.

- 123 [8] **CMS** Collaboration, R. Adolphi et al. *JINST* **0803** (2008) S08004.
- 124 [9] **CMS** Collaboration, G. L. Bayatian et al. CERN-LHCC-2006-001.
- 125 [10] G. P. Salam and G. Soyez *JHEP* **05** (2007) 086.
- 126 [11] **GEANT4** Collaboration, S. Agostinelli et al. *Nucl. Instrum. Meth.* **A506** (2003) 250.
- 127 [12] **CMS** Collaboration *CMS Physics Analysis Summary* **JME-07-002** (2008).
- 128 [13] **CMS** Collaboration *CMS Physics Analysis Summary* **JME-07-003** (2008).
- 129 [14] T. Sjostrand, L. Lonnblad, and S. Mrenna arXiv:hep-ph/0108264.
- 130 [15] Z. Nagy *Phys. Rev.* **D68** (2003) 094002.
- 131 [16] J. Pumplin et al. *JHEP* **07** (2002) 012.
- 132 [17] **CDF** Collaboration, T. Aaltonen et al. *Phys. Rev.* **D79** (2009) 112002.

DRAFT

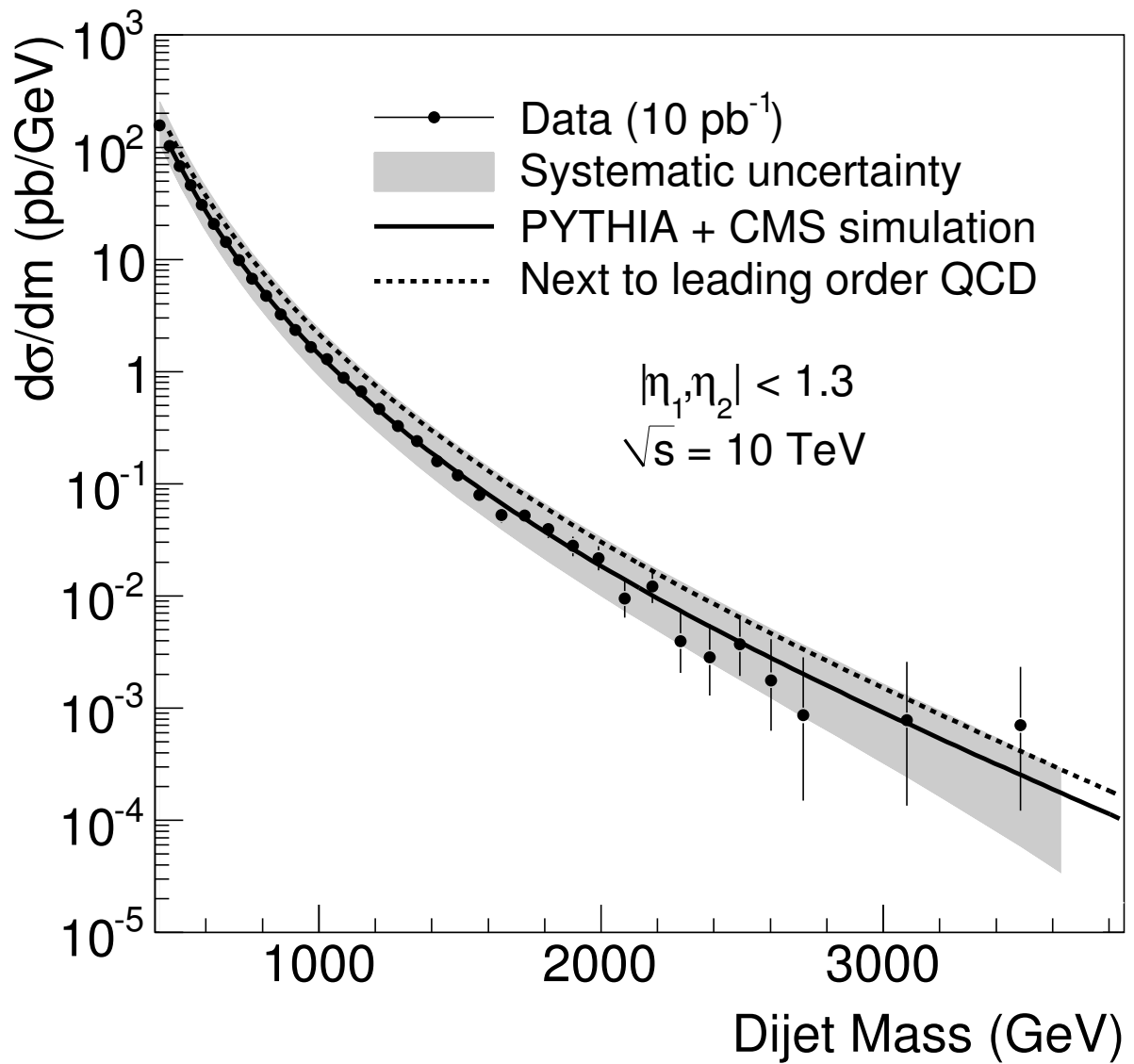


Figure 1: The dijet mass distribution (points) compared to a simulation of QCD and the CMS detector (solid curve) and a next-to-leading order QCD calculation (dashed curve). The band shows the systematic uncertainties on the data. WARNING: CMS DATA IN THIS FIGURE IS FAKE

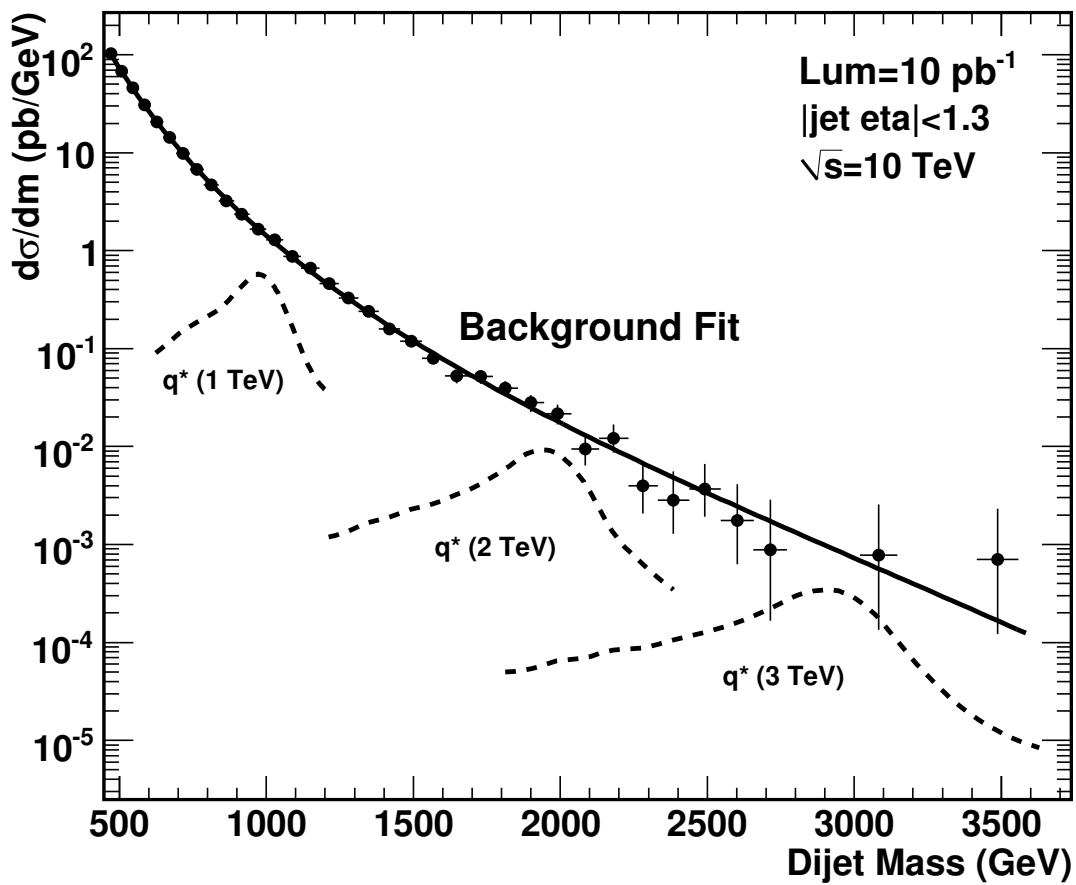


Figure 2: The dijet mass distribution (points) compared to a smooth background fit (solid curve) and to a simulation of excited quarks signals in the CMS detector (dashed curves).
WARNING: CMS DATA IN THIS FIGURE IS FAKE

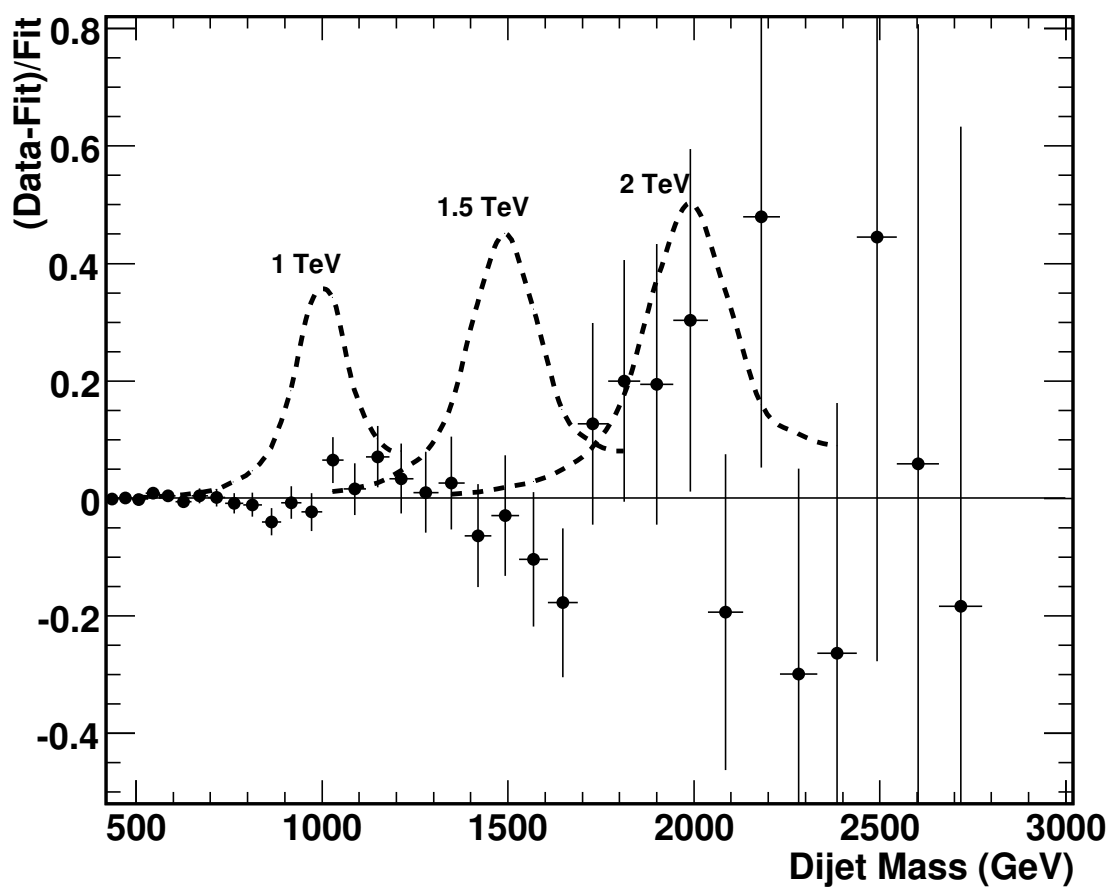


Figure 3: The fractional difference between the dijet mass distribution (points) and a smooth background fit (solid line) is compared to simulations of excited quark signals in the CMS detector (dashed curves). WARNING: CMS DATA IN THIS FIGURE IS FAKE

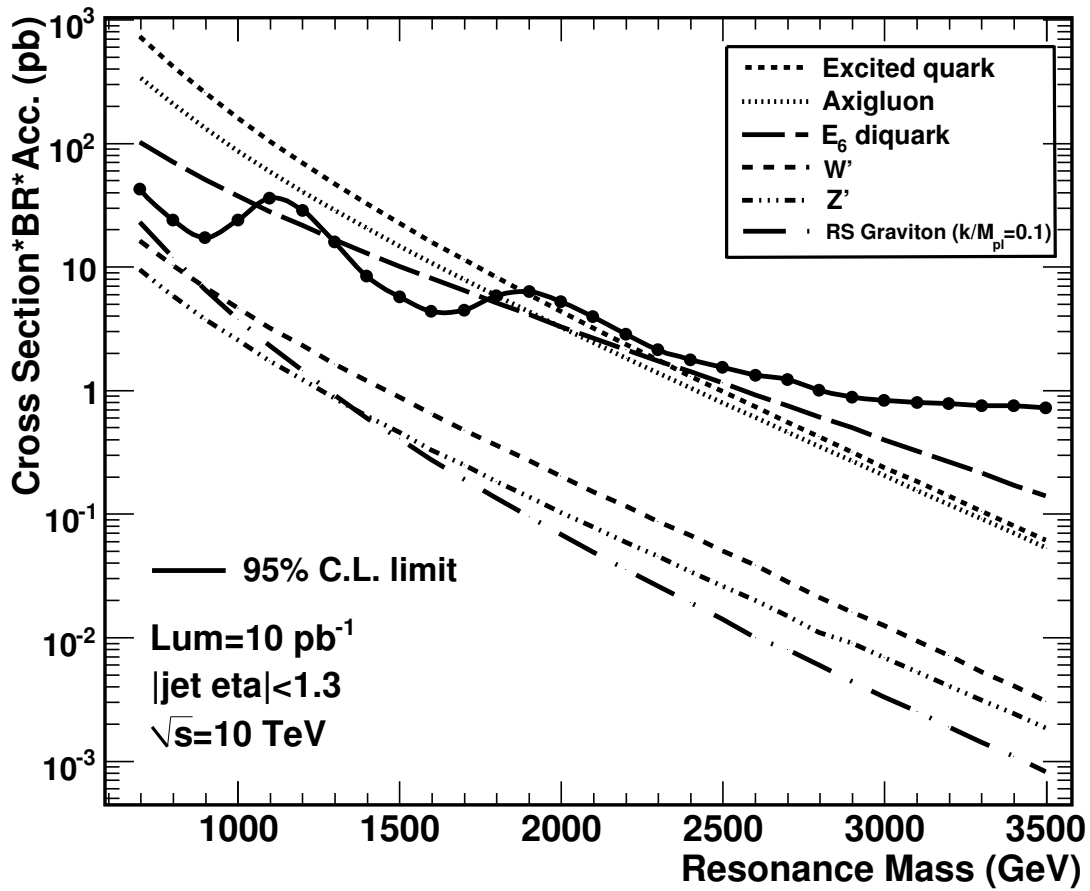


Figure 4: The upper limit on the cross section times branching ratio for new particles decaying to dijets (points) is compared to theoretical predictions for axigluons [1], flavor universal colorons [2], excited quarks [3], E_6 diquarks [4], Randall-Sundrum gravitons [6], and new gauge bosons W' and Z' [7]. The limit and theory curves require that both jets have pseudorapidity $|\eta| < 1.3$. WARNING: FROM FAKE DATA AND INCLUDING STATISTICAL UNCERTAINTIES ONLY

Table 1: As a function of new particle mass we list our 95% C.L. upper limit on cross section times branching ratio for narrow resonances decaying to dijets. The limit applies to the kinematic range where both jets have pseudorapidity $|\eta| < 1.3$ WARNING: FROM FAKE DATA AND INCLUDING STATISTICAL UNCERTAINTIES ONLY.

Mass (TeV/ c^2)	95% C.L. $\sigma \cdot B$ (pb)
0.7	42
0.8	24
0.9	17
1.0	24
1.1	35
1.2	29
1.3	16
1.4	8.3
1.5	5.7
1.6	4.3
1.7	4.5
1.8	5.8
1.9	6.3
2.0	5.3
2.1	3.9
2.2	2.8
2.3	2.1
2.4	1.8
2.5	1.5
2.6	1.3
2.7	1.2
2.8	1.0
2.9	0.88
3.0	0.83
3.1	0.80
3.2	0.79
3.3	0.78
3.4	0.76
3.5	0.73